JMEPEG (2016) 25:2307–2317
DOI: 10.1007/s11665-016-2051-2

1059-9495/$19.00

Effect of Double Aging Heat Treatment on the Short-Term Creep Behavior of the Inconel 718

Felipe Rocha Caliari, Kátia Cristiane Gandolpho Candioto, Antônio Augusto Couto, Carlos Ângelo Nunes, and Danieli Aparecida Pereira Reis

(Submitted March 30, 2015; in revised form February 18, 2016; published online April 22, 2016)

This research studies the effect of double aging heat treatment on the short-term creep behavior of the superalloy Inconel 718. The superalloy, received in the solution treated state, was subjected to an aging treatment which comprises a solid solution at 1095 °C for 1 h, a first aging step of 955 °C for 1 h, then aged at 720 and 620 °C, 8 h each step. Creep tests at constant load mode, under temperatures of 650, 675, 700 °C and stress of 510, 625 and 700 MPa, were performed before and after heat treatment. The results indicate that after the double aging heat treatment creep resistance is increased, influenced by the presence of precipitates γ′ and γ″ and its interaction with the dislocations, by grain size growth (from 8.20 to 7.23 ASTM) and the increase of hardness by approximately 98%. Creep parameters of primary and secondary stages have been determined. There is a breakdown relationship between $\dot{\varepsilon}_s$ and stress at 650 °C of Inconel 718 as received, around 600 MPa. By considering the internal stress values, effective stress exponent, effective activation energy, and TEM images of Inconel 718 double aged, it is suggested that the creep mechanism is controlled by the interaction of dislocations with precipitates. The fracture mechanism of Inconel 718 as received is transgranular (coalescence of dimples) and mixed (transgranular-intergranular), whereas the Inconel 718 double aged condition crept surfaces evidenced the intergranular fracture mechanism.

Keywords creep behavior, double aging, Inconel 718, TEM

1. Introduction

Materials applied in high temperature must be able to work in long-term with reliability, by keeping close to initial project dimensions, mechanical properties, and resistance to hot corrosion environment. The utilization of superalloys in high temperature and corrosive environments requires fully characterization of their mechanical properties under extreme temperature and stress levels. Inconel 718 is a nickel-based superalloy containing 5.0-5.5% niobium and composes the backbone of jet engines, both commercial and military. This superalloy is hardened by the precipitation of intermetallics compounds such as gamma prime (Ni_3[Al, Ti]-γ′) and gamma double prime (Ni_3Nb-γ″) (Ref 1, 2).

The phenomenon of creep on precipitation hardened superalloys and intermetallic materials has been studied by several authors (Ref 3-16). Studies have been done on standard and modified Inconel 718, regarding fatigue and stress rupture properties (Ref 17-21), which have shown the influence of niobium, titanium, and aluminum content on γ′ and γ″ phase stability and anti-phase boundary (APB) energy. However, few contributions have been done over the determination of stress exponent and activation energy, in order to fully characterize the creep controlling mechanism of double aged Inconel 718. In addition, the effect of aging conditions, specially the control of precipitation of delta phase (Ni_3Nb-δ orthorhombic) by increasing the solid solution treatment temperature and the respective effect on stress exponent and activation energy has not been studied yet.

Precipitation hardening alloys can exhibit a wide variation of values of stress exponent, and has been reported in the literature values between 5 and 15 (Ref 6, 16). The precipitates γ′ and γ″, which promote the mechanical resistance of Inconel 718, work mainly as obstacles for dislocation and grain boundary sliding, and as mentioned by Singhal and Vaidya grain boundaries also play as a dislocation source in precipitation hardened alloys (Ref 4). A singularity of alloys hardened by precipitation of secondary phases is the strong break between creep rate and stress in low stress values, where the high dependence of the creep rate relative to the applied stress is replaced by low dependence (Ref 6). Zhou and Parker (Ref 22) studied the effects of the high stress on creep behavior of precipitation hardened zinc-based alloy. They pointed that high stress regime is evidenced by high stress exponent values and that within this regime the σ_p (stress due to precipitation hardening) corresponds to a threshold stress, which is related to the Orowan mechanism.

The application of aging heat treatment usually comprises two steps: solid solution treatment and aging. The solid solution temperature must be carefully chosen because at temperatures close to the solvus line creep resistance obtained is increased (Ref 1). Kuo et al. reported (Ref 23) the increasing temperature of the solid solution used over time, in order to dissolve

Dedicated to the memory of Prof. Carlos de Moura Neto.

Felipe Rocha Caliari and **Danieli Aparecida Pereira Reis**, ITA – Instituto Tecnológico de Aeronáutica, São José dos Campos SP, Brazil and UNIFESP - Universidade Federal de São Paulo, São José dos Campos, SP, Brazil; **Kátia Cristiane Gandolpho Candioto** and **Carlos Ângelo Nunes**, EEL-USP – DEMAR, Universidade de São Paulo, Lorena, SP, Brazil; and **Antônio Augusto Couto**, IPEN – Instituto Pesquisas Energéticas e Nucleares, São Paulo, SP, Brazil. Contact e-mail: felipercaliari@yahoo.com.br.

Table 1 Tensile properties of Inconel 718, before and after heat treatment

Inconel 718	Temperature, °C	YS, MPa	UTS, MPa	EL, %	RA, %
AR	650	355.35	676.32	12.55	28.32
	700	421.48	588.56	5.51	12.27
DA	650	1062.61	1130.24	6.49	6.77
	700	974.31	1006.50	4.83	2.45

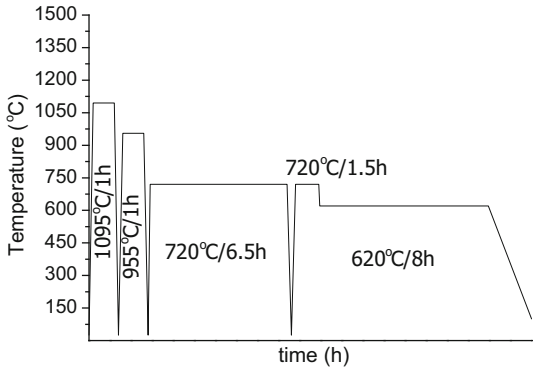

Fig. 1 Double aging heat treatment applied on Inconel 718

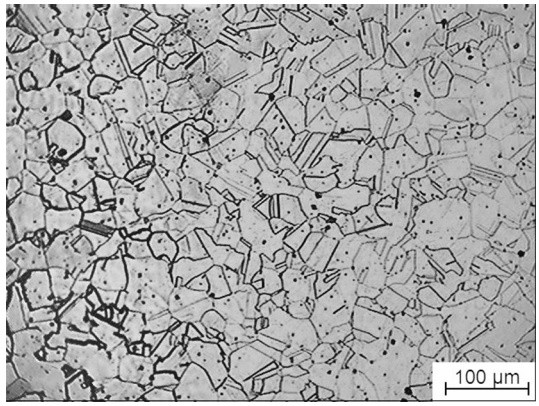

Fig. 2 Optical micrograph of Inconel 718 as-received

detrimental phases such as delta, μ, and Laves. This research aims to study the effect of double aging heat treatment on short-term creep properties of the superalloy Inconel 718 by correlating the microstructural aspects to the creep parameters.

2. Experimental Procedure

Superalloy Inconel 718 was obtained via vacuum induction melting and vacuum arc remelting (VIM/VAR) process, solutioned (1026 °C/1.5 h) by Multialloy Co. (São Paulo, Brazil), with the following composition (wt.%): Ni = 54.47%; Cr = 18.94%; Fe = 17.99%; Nb = 5.89%; Mo = 1.35%; Ti = 1.05% and Al = 0.27%. The as-received (solutioned) and double aged conditions in this work are identified as AR and DA, respectively. Double aging heat treatment followed the steps: (i) Solution treatment of 1095 °C for 1.0 h/AC, and (ii) aging at 955 °C for 1 h/AC (iii) aging at 720 °C for 6.5 h/FC + 720 °C for 1.5 h/FC + 620 °C for 8.0 h/FC (Fig. 1). The heat treatment was conducted in a Lindberg/Blue M tubular furnace (100 V/50 A/50 kW), using argon atmosphere. Specimens were encapsulated in a quartz tube during heat treatment to avoid oxidation. The hardness values of all samples were determined using a Buehler Micromet equipment with a load of 25 kgf for 15 s, 10 measurements. Hot tensile tests were conducted at 650 and 700 °C in an Instron 3382 100 kN Metal Package equipped with Instron's Series IXTM/s software with deformation rate of 0.5 mm/min (2×10^{-4} s^{-1}) according to ASTM E21 (Ref 24). The tensile properties such as yield stress (YS), ultimate tensile stress (US), elongation (EL), and reduction of area (RA) for the Inconel 718 AR and DA are described in Table 1. Based on the tensile properties for each condition, the creep stress values were determined. Constant load creep tests were conducted according to ASTM E139-11 (Ref 25), in a standard Mayes creep machine. The Inconel 718

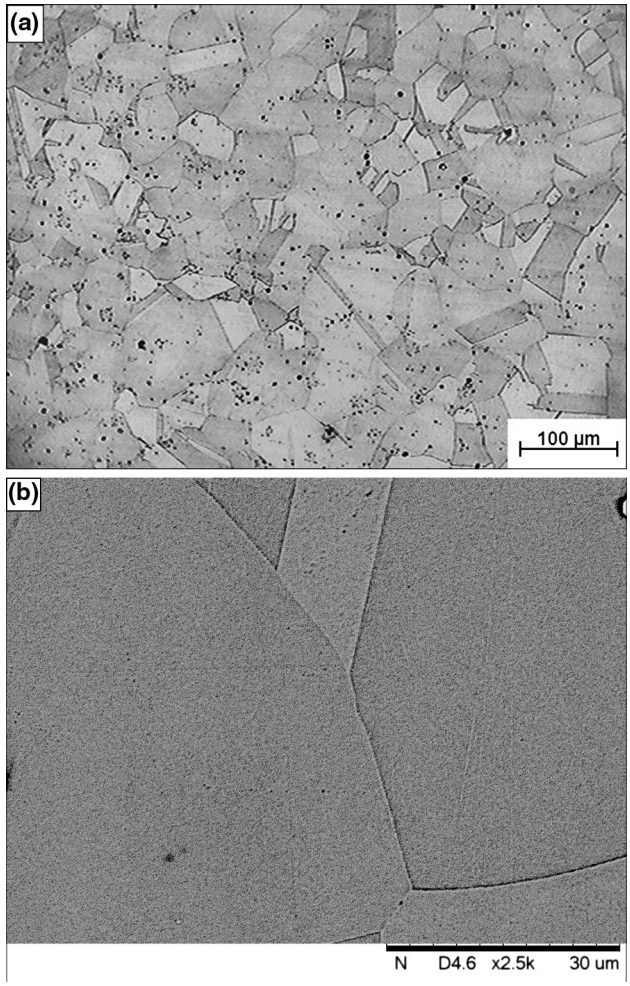

Fig. 3 Micrographs of Inconel 718 double aged, (a) OM general view and (b) SEM detail of grain boundary

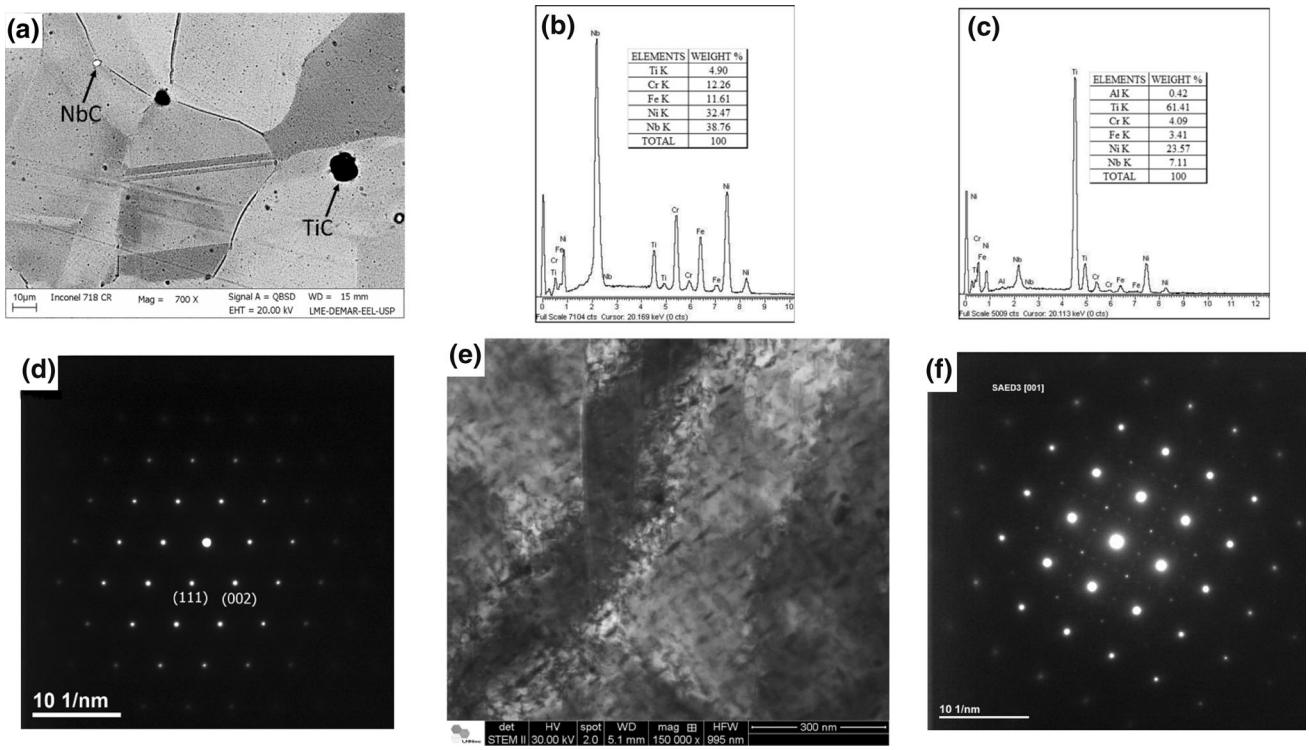

Fig. 4 Microstructure of Inconel 718: (a) detail of the large-scale precipitates on the AR condition with EDS of respective (b) clear precipitate and (c) dark precipitate. A SAD pattern (d) taken from the [001] zone axis of Inconel 718 AR. STEM image of the double aged microstructure showing (e) γ' and γ'' precipitates and (f) SAD pattern of Inconel 718 DA taken from [001] axis

Table 2 Comparison of the creep parameters for investigated conditions

T, °C	σ, MPa	Inconel 718	t_p, h	$\dot{\varepsilon}_s$, 1/h	t_f, h	ε_f
650	319	AR	48	3.7E−06	(*)	(*)
		DA	92	3.8E−07	(*)	(*)
	510	AR	156.00	1.76E−05	398.50	0.058
		DA	90.00	4.43E−07	(*)	(*)
	625	AR	1.05	3.82E−04	10.43	0.175
		DA	48.00	2.84E−05	230.80	0.013
	700	AR	0.02	5.83E+00	0.05	0.302
		DA	8.00	4.58E−05	58.00	0.007
675	510	AR	22.00	4.64E−05	77.75	0.023
		DA	90.00	8.36E−06	297.00	0.011
	625	AR	0.02	1.28E−01	0.08	0.169
		DA	18.00	9.96E−05	45.00	0.007
	700	AR	0.01	1.19E+01	0.03	0.281
		DA	1.53	3.45E−04	11.23	0.008
700	510	AR	1.67	3.18E−04	10.42	0.011
		DA	3.00	9.89E−05	41.40	0.009
	625	AR	0.01	1.06E+01	0.03	0.124
		DA	1.07	3.23E−04	7.95	0.010
	700	AR	0.01	1.33E+01	0.03	0.127
		DA	0.33	1.74E−03	2.95	0.011

(*) Test interrupted before rupture

AR and DA were evaluated under stress range of 510-700 MPa and temperatures 650, 675, and 700 °C (T_h is approximately 0.49, 0.51, and 0.52, respectively). Test samples with a gage length of 18.5 mm and a diameter of 3.0 mm were used for all tests. Each tensile and creep test was repeated twice. Inconel 718 as-received, double aged and selected samples after the creep tests were analyzed in a OM Axio Scope A.1 Zeiss, a SEM LEO 1450 VP equipped with an EDS detector from Oxford Instruments, FEI Helios Nanolab 660 in STEM mode at 30 kV, and a JEOL2100 transmission electron microscope

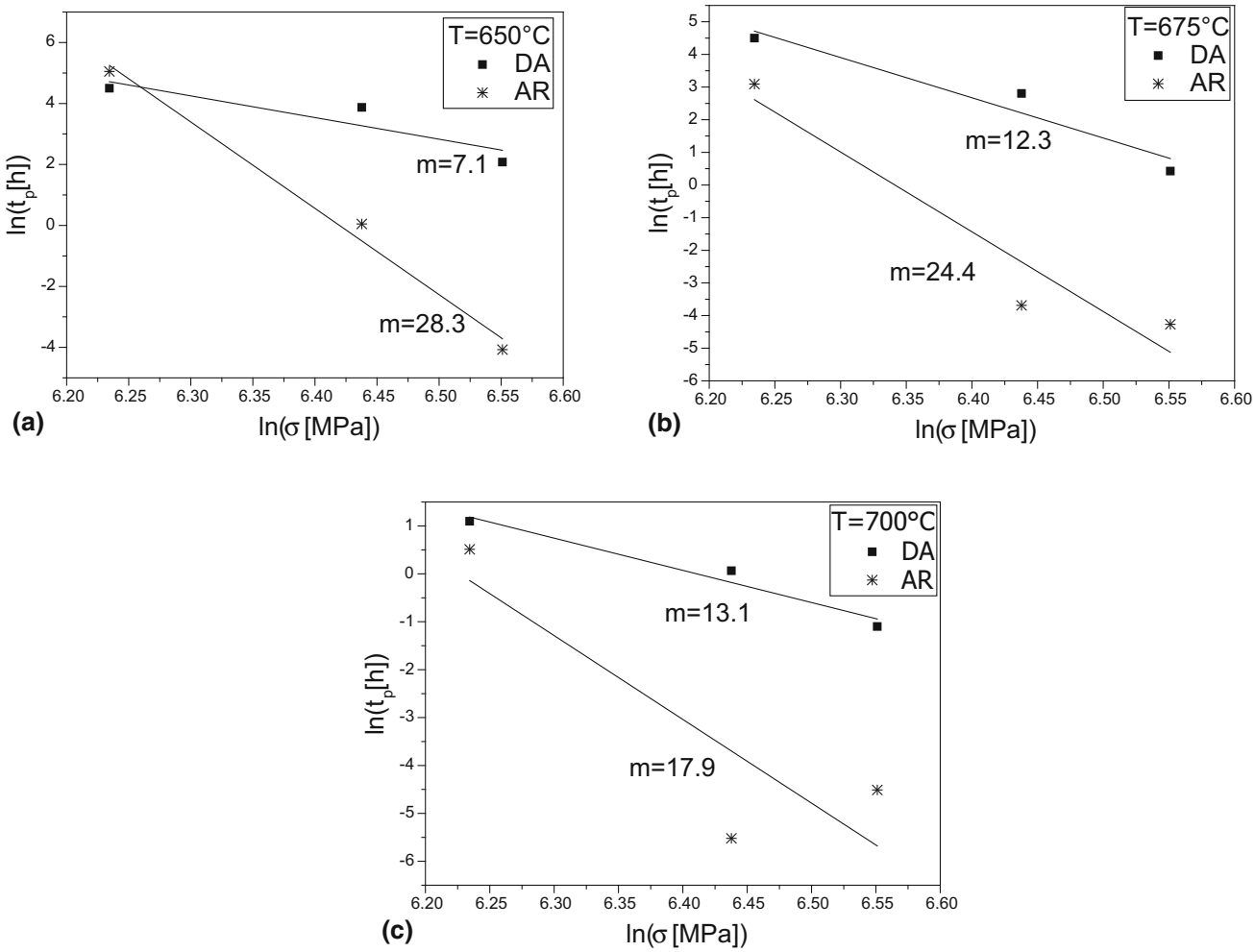

Fig. 5 Relationship between primary creep time and apparent stress at (a) 650 °C, (b) 675 °C, and (c) 700 °C

(TEM) operating at 200 kV. The samples were prepared for OM and SEM analysis following conventional metallographic techniques and etched with a glyceregia solution, and STEM/TEM samples preparation was followed by cutting sections (3 mm of diameter) perpendicular from the tensile axis, grinding until 50-60 μm, then electropolished at 20 V DC in a solution of 90% methyl alcohol and 10% perchloric acid at a temperature of −10 °C in a Tenupol 5. TEM samples were analyzed using a two-beam technique with zone axis of [001]. The qualitative phase analysis of Inconel 718 AR/DA before and after creep tests was performed by x-ray diffraction (XRD) in a Rigaku, Ultima IV diffractometer, operating at 30 mA and 40 kV.

3. Results and Discussion

3.1 Microstructural Characterization Before and After DA Heat Treatment

Microstructural images obtained via optical microscopy for AR and DA conditions are shown in Fig. 2 and 3, respectively. Before the heat treatment, the superalloy shows a gamma (γ) matrix based on Ni-Cr-Fe with secondary particles clustering—large-scale precipitates (see Fig. 4a-c) based on NbC, TiC, and delta phases derived from a non-controlled precipitation process (Ref 26), ASTM grain size (ASTM E112-10) of 8.20 and hardness of 202 ± 10 HV.

After the double aging heat treatment, the Inconel 718 shows a homogeneous distribution of secondary particles as well as ASTM grain size of 7.23 and hardness of 401 ± 23 HV. The solution treatment temperature of 1095 °C (standard solid solution treatment temperature is 980 °C, per AMS 5662) used in this work successfully solved the large-scale precipitates found on the initial microstructure (see Fig. 3a), also no precipitation was observed on the grain boundary (Fig. 3b). TEM selected area diffraction (SAD) pattern of Inconel 718 is illustrated on Fig. 4(d) (as-received) and 4(f) (double aged). According to the STEM image (Fig. 4e) and SAD pattern, the Inconel 718 double aged (Fig. 4f) possesses nano-scale γ′ and γ″ precipitates, whereas the SAD pattern of AR material (Fig. 4d) does not indicate precipitation of γ′ and γ″.

3.2 Short-Term Creep Properties

Initially hot tensile tests were performed on Inconel 718 specimens in both AR and DA conditions for the temperatures of 650 and 700 °C. From the Yield Strength (YS) and Ultimate Tensile Strength (UTS) values, the creep load was established.

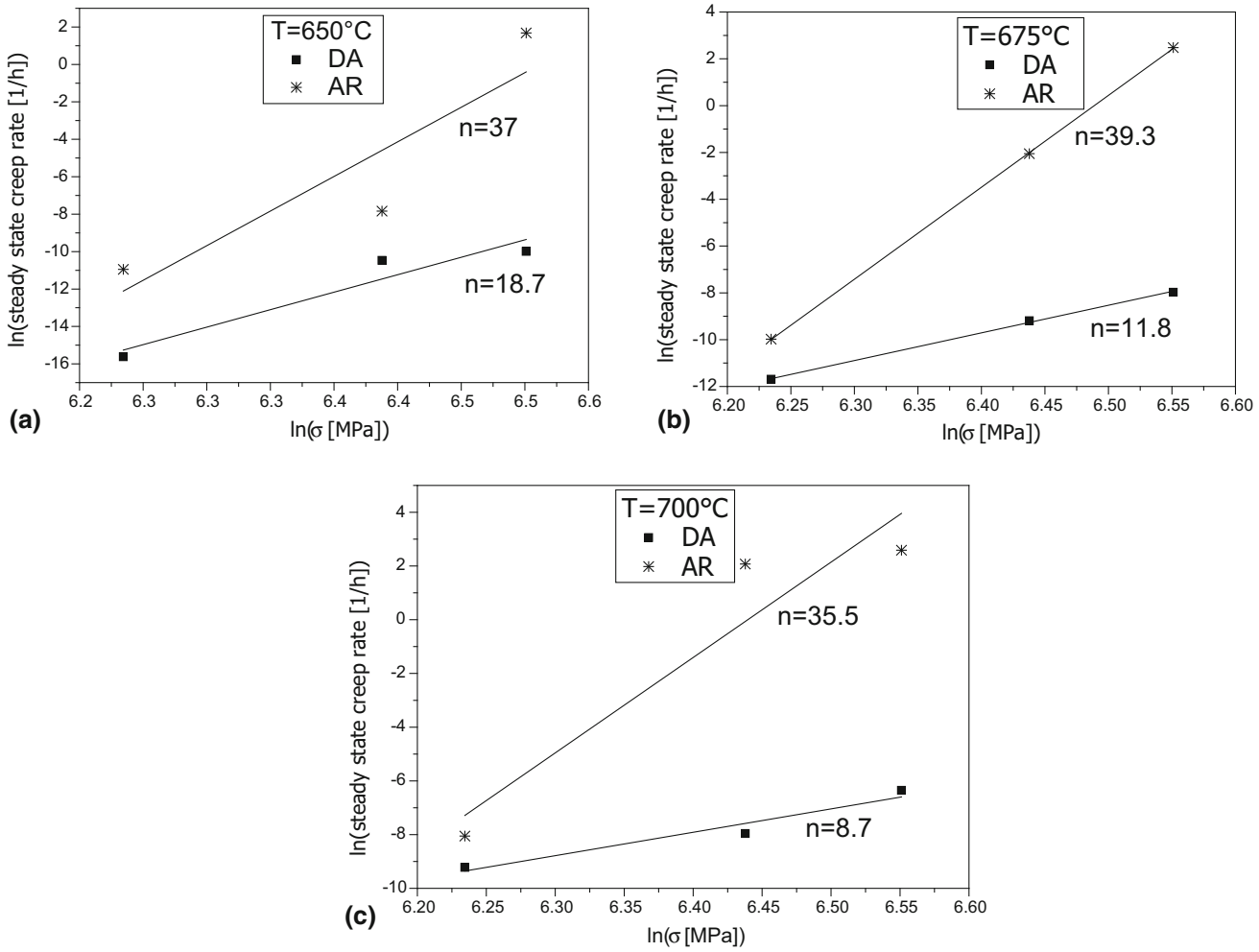

Fig. 6 Apparent stress exponent of Inconel 718 at (a) 650 °C, (b) 675 °C, and (c) 700 °C

Additionally, the hot tensile test results show the higher mechanical resistance of double aged condition.

Creep parameters were determined from curves and summarized in Table 2. An increase in creep resistance can be noticed by comparing the time to failure (t_f), primary creep time (t_p), and steady-state creep rate ($\dot{\varepsilon}_s$) after the double aging treatment.

The logarithm correlation of Eq 1 between primary creep time and stress is detailed in Fig. 5 (Ref 27):

$$t_p = A\sigma_A^{-m}, \quad \text{(Eq 1)}$$

where A is a constant related to the microstructure, m is the creep stress exponent in the primary stage, and σ_A is the applied stress. The apparent stress exponent for primary creep stage ranged between 17.9 and 28.3 for Inconel 718 AR, whereas on the DA condition the values obtained were between 7.1 and 13.1, as represented in Fig. 5. From the results obtained one can notice that the AR condition is more sensitive to the stress than the aged condition because, in this case, higher exponent values lead to higher creep deformation.

The steady-state creep rate can be correlated with the apparent stress using the Eq 2 from the set of data collected in Table 2 (Ref 28):

$$\dot{\varepsilon}_s = B\sigma_A^{n_a}, \quad \text{(Eq 2)}$$

where B is a constant inherent to the microstructure, n_a is the apparent creep stress exponent for the secondary stage. The results of apparent stress exponent for the secondary stage of creep, see Fig. 6, are found to be between 35.5 and 39.3 for AR condition, while for DA condition the values ranged from 8.7 to 18.7. The lower values of apparent stress exponent in secondary stage, for the DA condition, are related to the lower dependence of the steady-state creep rate in relation to the stress values due to the increase of internal stress, which is related to the γ' and γ'' particle-dislocation interaction, and the decrease of grain boundary area due to grain growth. This particle-dislocation interaction is observed on Fig. 7, where Fig. 7(a) illustrates the dislocation movement during creep tests on Inconel 718 AR, and Fig. 7(b) and (c) shows respectively the particles blocking the dislocation movement as well as particle shearing, during creep tests on the Inconel 718 double aged.

By correlating the AR values of the steady-state creep rate, for the same temperature/stress regime, one can notice the $\dot{\varepsilon}_s$ values are close until 510 MPa, but the difference between them increase with increasing stress. Figure 8 supports this observation, whereas it is shown a sharp change on the $\dot{\varepsilon}_s$-σ

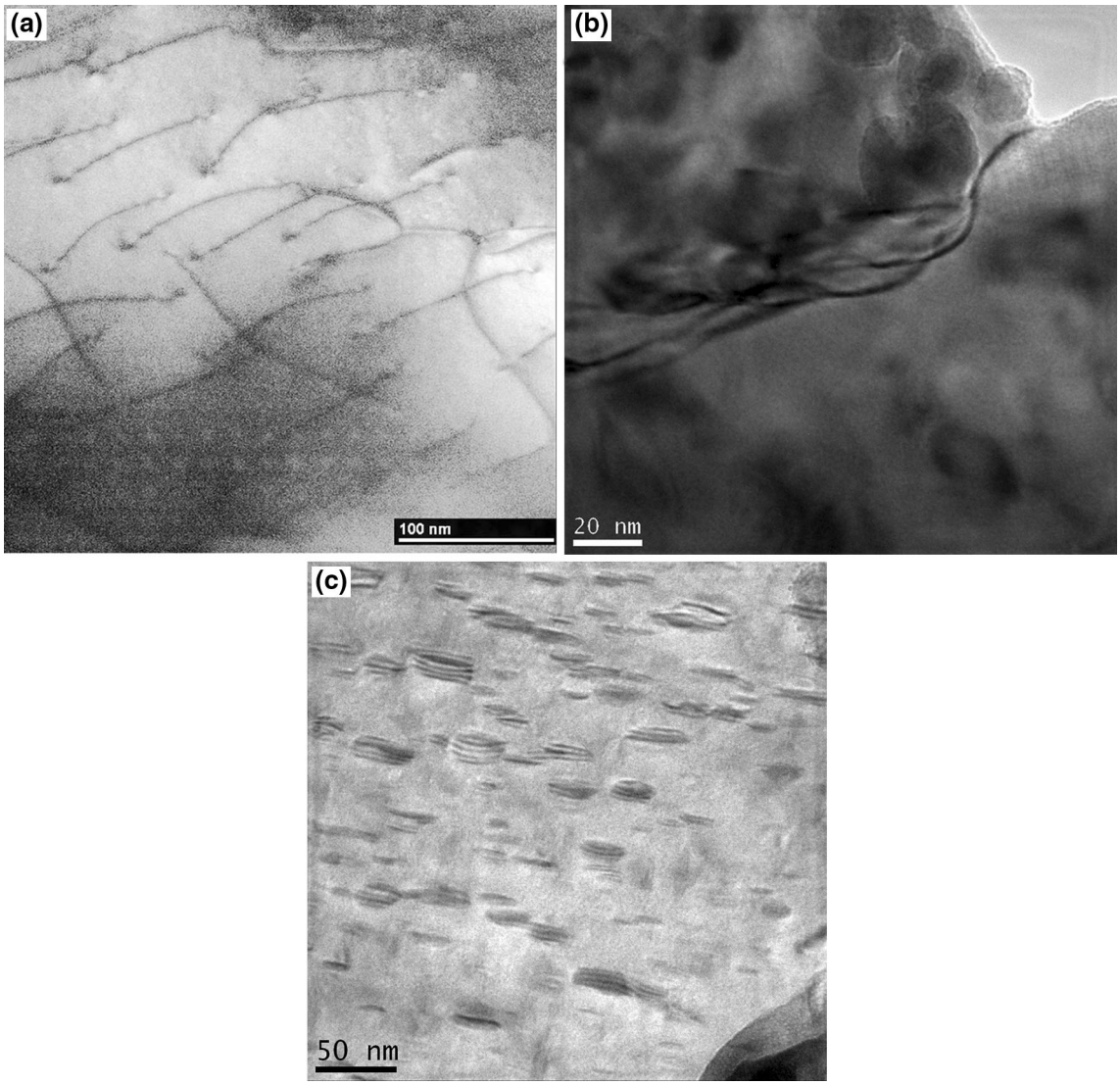

Fig. 7 TEM micrographs of crept specimens, (a) dislocation on Inconel 718 AR, (b) precipitates blocking dislocation movement on Inconel 718 DA (c) particle shearing after creep testing

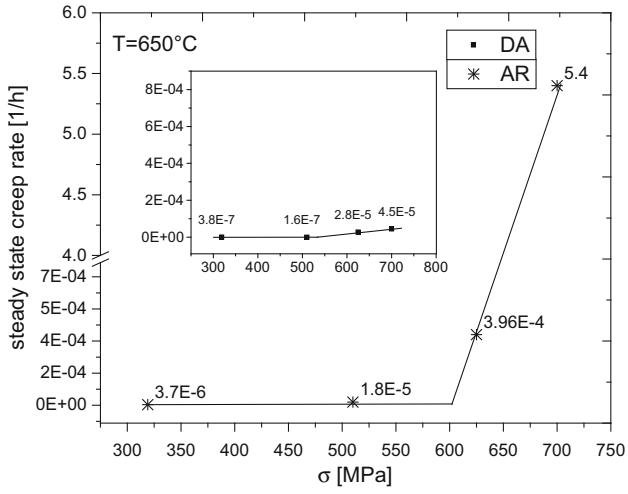

Fig. 8 Relationship between stress-secondary creep rate for AR and DA conditions

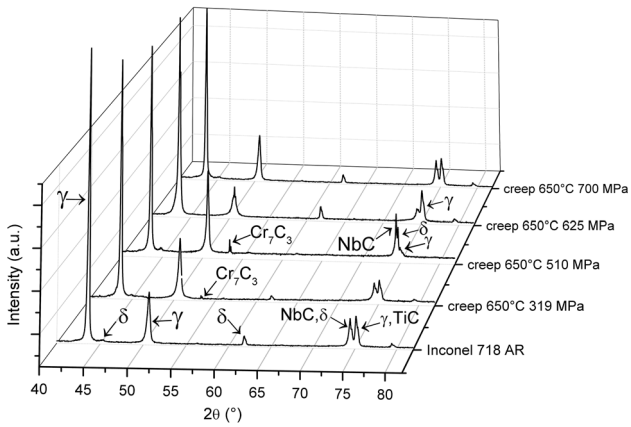

Fig. 9 XRD pattern of AR samples at 650 °C, for different applied stresses

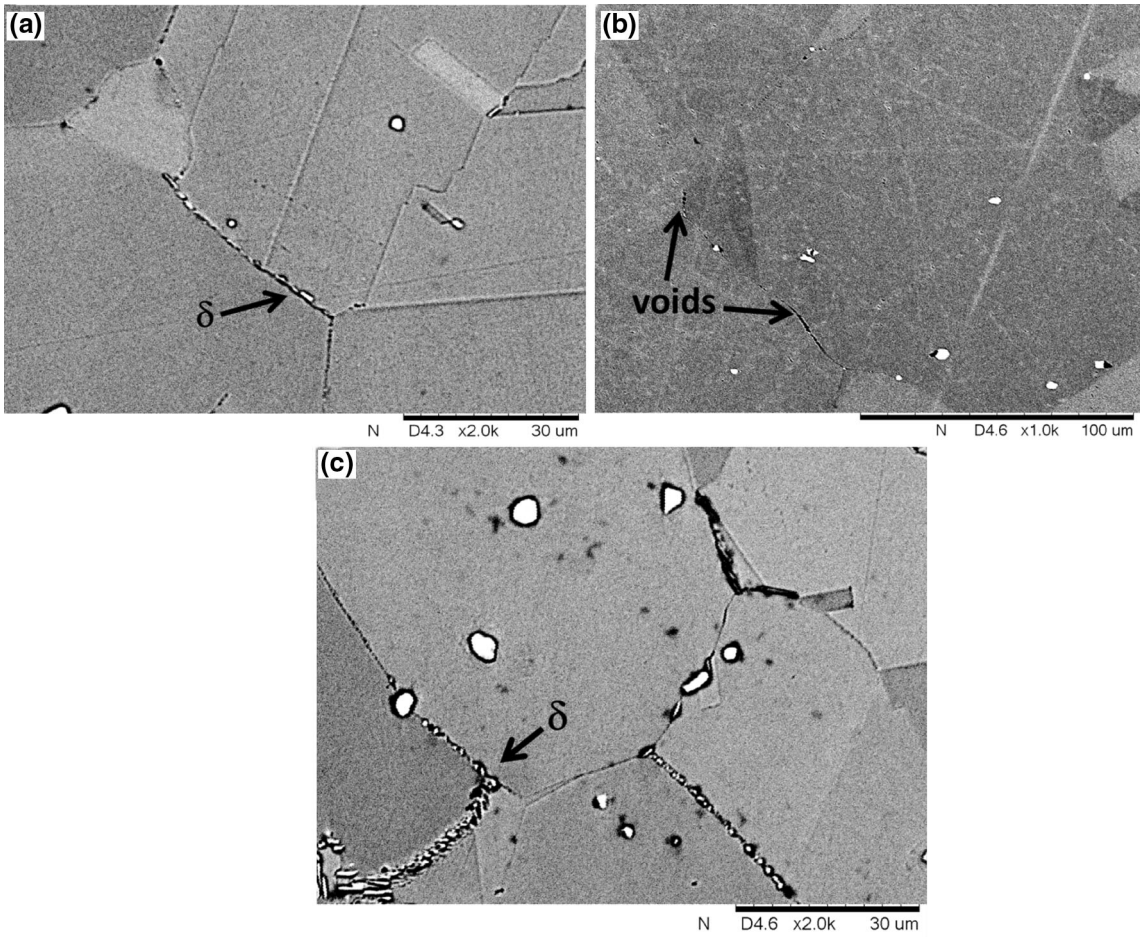

Fig. 10 Microstructures of Inconel 718 DA after creep test, (a) sample tested at 650 °C and 625 MPa, (b) sample at 700 °C and 510 MPa and (c) 700 °C and 625 MPa

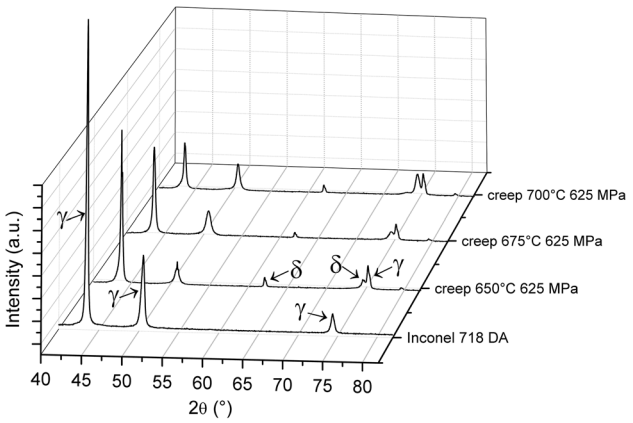

Fig. 11 XRD pattern of DA samples at 625 MPa, for different applied temperatures

relationship near 600 MPa for AR condition (at 650 °C), which may be related to precipitation during creep tests at 319 and 510 MPa. The x-ray diffraction pattern from AR specimens at 650 °C and 319-700 MPa (Fig. 9) substantiates the abovementioned precipitation during creep tests, where the presence of Cr_7C_3 (orthorombic) was detected only on specimens tested at 319 and 510 MPa. According to the Helmholtz free energy

Table 3 Apparent and effective stress exponents for aged Inconel 718

Temperature, °C	Applied stresses, MPa	n_a	n_e
650(a)	620, 670, 695	10.00	2.3
650(b)	510, 625, 700	18.66	…
670(a)	620, 670, 695	10.40	5.9
675(b)	510, 625, 700	11.80	…

(a) Data originally published in Han and Chaturvedi (Ref 32]. (b) Data from current work

calculation made by Kaplan et al. (Ref 29), the orthorhombic—Cr_7C_3 is rather stable than hexagonal structure above 200 °C. The formation of such carbide coincides with creep tests that operated for longer times (319 and 510 MPa operated for 180 and 700 h, respectively). This carbide (Ref 30) is associated to embrittlement when they agglomerate on the grain boundary, and reduce grain boundary sliding (Ref 31). This precipitation observed during creep tests (for AR specimens tested at 650 °C, 319 and 510 MPa) probably contributed to the low creep strain values on AR condition. By increasing the creep stress applied on the Inconel 718 AR, one can observe the respective increase of the creep strain-rate, creep strain and

decrease of time to the fracture. At this point the relationship of $\dot{\varepsilon}_s$-σ given by Eq 2 is no longer valid, and finally the power law breaks down. At high stress the results of creep tests on Inconel 718 AR showed that not only creep deformation but also the bulk plasticity contributes on deformation, as can be concluded from the high levels of $\dot{\varepsilon}_s$.

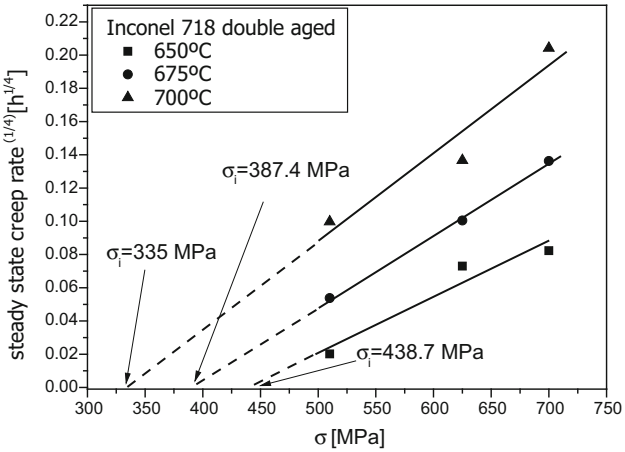

Fig. 12 Determination of internal stress of Inconel 718 double aged at 650, 675, and 700 °C

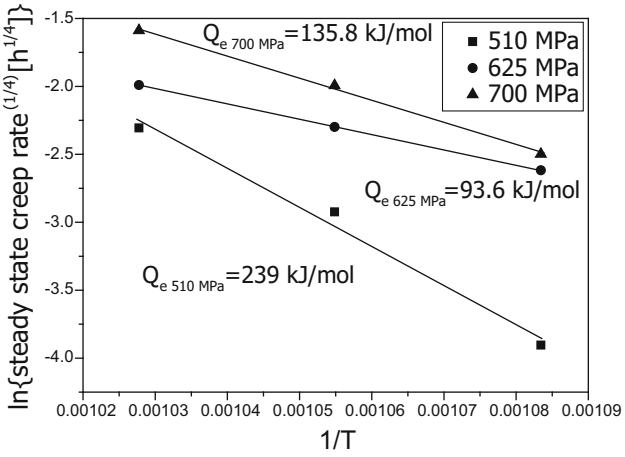

Fig. 14 Values of effective activation energy for creep deformation, at 510, 625, and 700 MPa

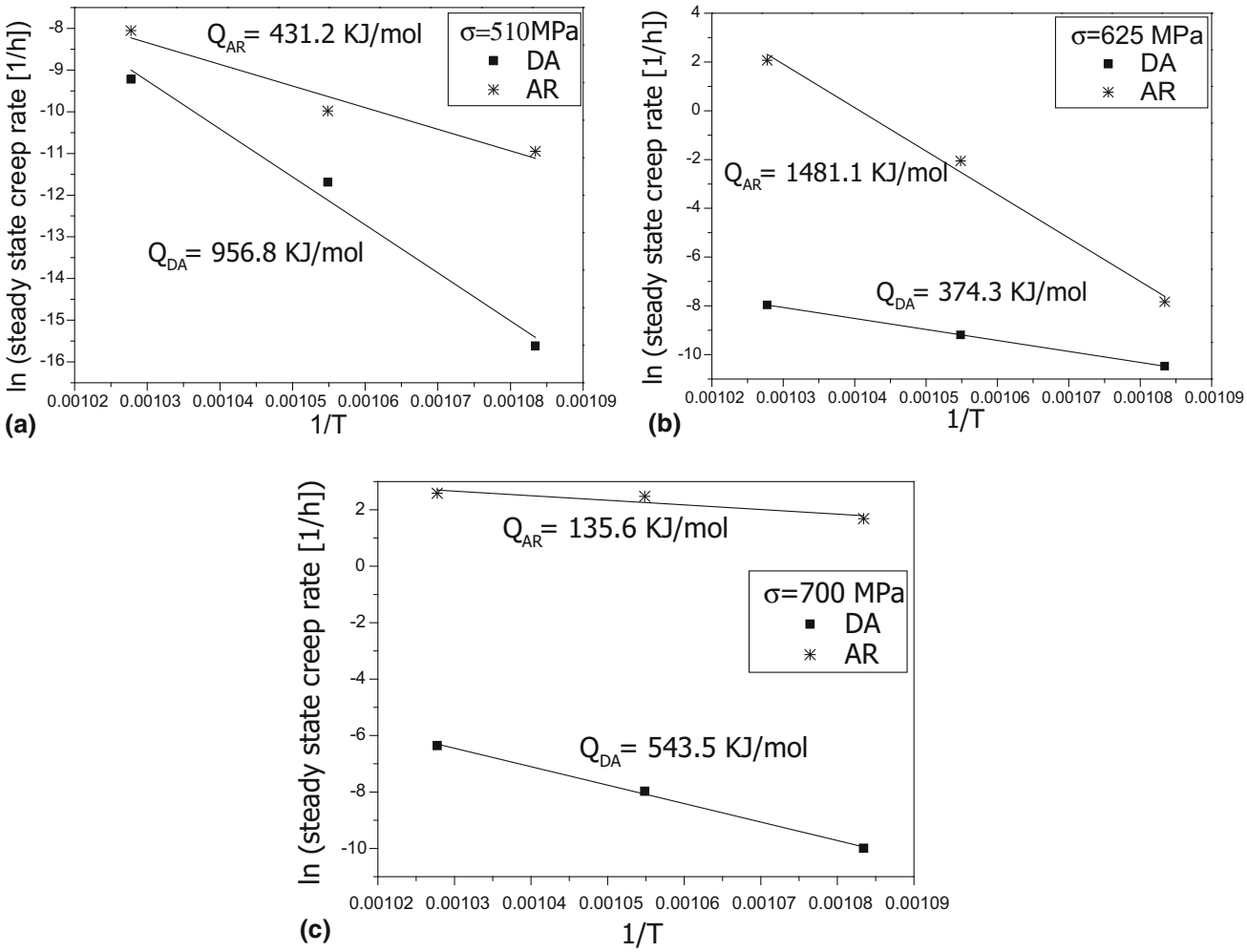

Fig. 13 Values of apparent activation energy for creep deformation, at (a) 510, (b) 625, and (c) 700 MPa

As for the DA condition, Fig. 8 does not indicate a breakdown on $\dot{\varepsilon}_s$-σ relationship within the range of 319-700 MPa (at 650 °C), and obeys the power-law creep with effective stress exponent of 4, as proposed by Lagneborg and Bergman (Ref 6). Moreover, it seems that the combined increase of stress and temperature compromises the microstructural stability and leads to early failure. Figure 10 represents the microstructure of DA specimens tested at (a) 650 °C and 625 MPa, (b) 700 °C and 510 MPa, and (c) 700 °C and 625 MPa, which compared to the initial microstructure (Fig. 3) shows precipitates and voids along the grain boundary. XRD pattern of Inconel 718 DA specimens (Fig. 11) indicates the presence of phase δ after creep tests, differently from the initial condition.

In order to evaluate and compensate the effect of internal stress on the stress exponent value, steady-state creep rate and stress can be correlated by using Eq 3 (Ref 28):

$$\dot{\varepsilon}_s = B(\sigma_A - \sigma_i)^{n_e}. \quad \text{(Eq 3)}$$

Han and Chaturvedi (Ref 32) studied the effect of internal stress (σ_i) on Inconel 718 conventionally aged using the consecutive stress reduction method, and calculated the effective stress exponent (n_e) of 2.3 ± 0.3, for the temperature of 650 °C, and 5.9 ± 1.9, for the temperature of 670 °C, with an applied stress between 620 and 695 MPa (see Table 3). Lagneborg and Bergman (Ref 6) developed studies of stress and creep rate relationship, and found that the transition from high to low stress sensitivity is associated to stress exponent of $n \sim 4$ on precipitation hardened alloys, noticing that their study encompassed mostly laboratory melted alloys. The authors (Ref 6) also describe the low sensitivity of stress/creep rate, in relation to the chemical composition and characteristics of the precipitate dispersion. One can realize that the effective stress exponent found by Han and Chaturvedi (Ref 32) at 650 °C is smaller compared to the one reported by Lagneborg and Bergman (Ref 6), and larger at 675 °C. This discrepancy is due to difference in the stress range applied, where the range studied by (Ref 32) is greater than the range surveyed by (Ref 6).

Assuming the value of $n_e = 4$ as a good approximation of effective stress exponent for this study, the values of internal stress can be determined by plotting $\dot{\varepsilon}_s^{\frac{1}{n_e}}$ versus applied stress, as shown in Fig. 12. The values of internal stress obtained are 438.7, 387.4, and 335 MPa for 650, 675, and 700 °C, respectively. One may notice that as the temperature is increased the internal stress is decreased, which is in agreement to the results obtained by Chen and Chaturvedi (Ref 33). Since γ'' is the main strengthening phase on Inconel 718, the transformation between the metastable γ'' and stable δ above 650 °C (Ref 34, 35) may contribute to the reduction internal stress.

In order to fully understand the creep behavior of Inconel 718 double aged, the activation energy for creep can be calculated by using Eq 3 (Ref 27):

$$\dot{\varepsilon}_s = B\sigma_A^{n_a} e^{-\left(\frac{Q_a}{RT}\right)}, \quad \text{(Eq 4)}$$

where R is the constant gas (8.31 J/mol K), Q_a is the apparent activation energy for creep deformation (Fig. 13). A reduction of 43% was observed on the activation energy calculated for DA condition and 68% for AR condition, as the applied stress is increased from 510 to 700 MPa. Both conditions of Inconel 718 show sensitivity of activation energy with the change on the applied stress. The values of activation energy should be close to the self-diffusion. Activation energy value for self-diffusion (Q_{sd}) of the solid solution Ni-20Cr heat treated has been reported by Venkataraman and Cosandey (Ref 36), to be around 295 kJ/mol. Considering only the DA condition, with the Q_a ranging between 374.6 and 956.8 kJ/mol, one may observe that the calculated values are above the one for Q_{sd}. This is related to the internal stress on Inconel 718 DA. By considering the σ_i value on activation energy calculation, it is necessary to use Eq 5 (Ref 27):

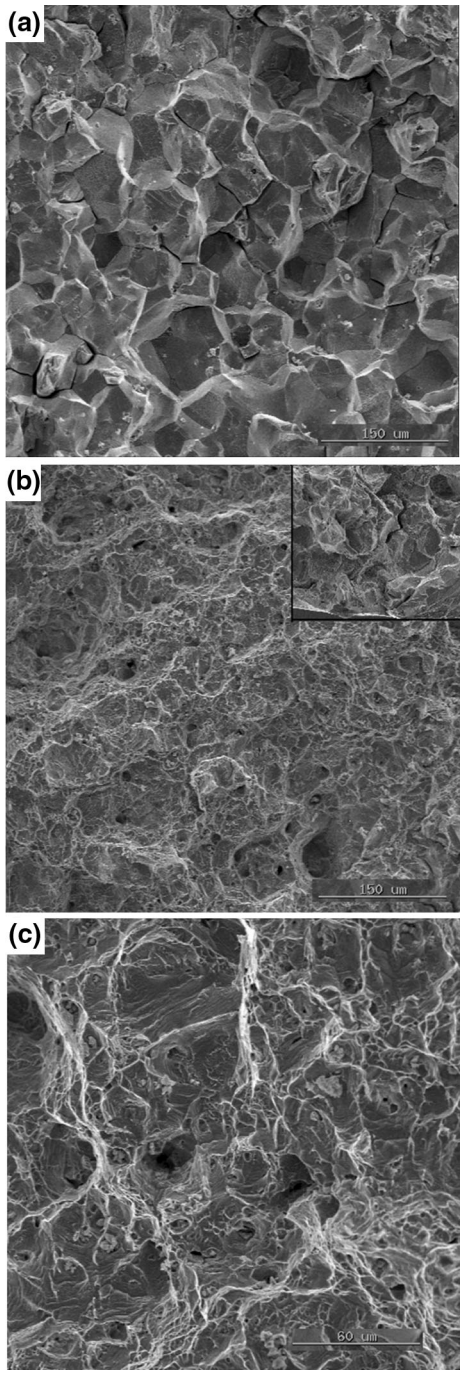

Fig. 15 Fracture surfaces of Inconel 718 AR crept at (a) 650 °C and 510 MPa, (b) 650 °C and 625 MPa, and (c) 700 °C and 625 MPa

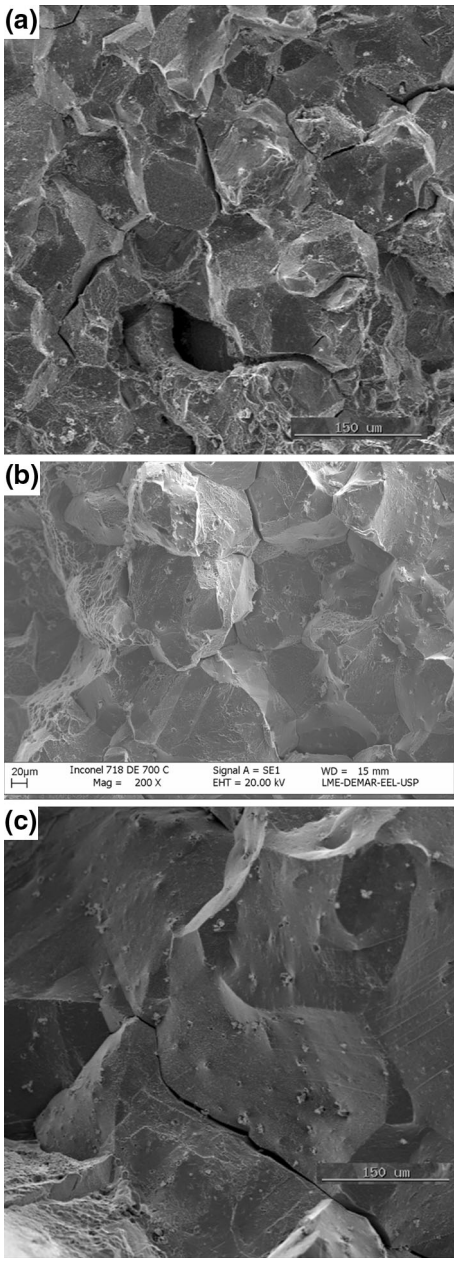

Fig. 16 Fracture surfaces of Inconel 718 DA crept at (a) 650 °C and 625 MPa, (b) 700 °C and 510 MPa, and (c) 700 °C and 625 MPa

$$\dot{\varepsilon}_s = B(\sigma_A - \sigma_i)^{n_e} e^{-\left(\frac{Q_e}{RT}\right)} \quad \text{(Eq 5)}$$

where Q_e is the effective activation energy for creep deformation. Figure 14 shows the values of Q_e calculated, considering the compensation of internal stress. Here one may notice that all values of effective activation energies are below Q_{sd}, also the value of Q_e at 510 MPa is close to the one reported by Chen and Chaturvedi (Ref 33). As evidenced by Fig. 7(c), the particle shearing controls the deformation of Inconel 718 DA; moreover, one can notice that the values of Q_e decrease with increasing stress.

Therefore, with the values of n_e, Q_e, σ_i, and TEM images of Inconel 718 DA, it is suggested that the controlling mechanism of creep deformation is the dislocation-precipitate interaction, controlled by the particle shearing.

3.3 Fracture Surface Analysis

The images of fracture surface obtained via secondary electrons mode (SEM) support the creep behavior aforementioned. Figure 15(a) shows the creep fracture of AR condition at 650 °C and 510 MPa, clearly representing an intergranular fracture. Figure 15(b) shows that for the AR condition tested at 650 °C and 625 MPa, fracture mode was mixed because both dimples (transgranular) and intergranular fractures are observed. The failure mode of AR condition tested at 700 °C and 625 MPa (Fig. 15c) was due to coalescence of dimples, also one may notice at the bottom of the cavity the presence of precipitates. Figure 16(a)-(c) shows that Inconel 718 DA failure mode is the intergranular creep fracture.

4. Conclusions

Distinct creep behavior is obtained by the calculation of apparent stress exponent and activation energy of Inconel 718 in the AR and DA conditions, both submitted to constant load creep tests. The double aging heat treatment conferred resistance to the Inconel 718 mainly by the precipitation of γ'', which is supported also by hot tensile tests results. The creep parameters calculated for the primary stage of creep deformation also show an increased resistance after heat treatment. The creep life of the as-received condition has a major influence on the applied stress, and there is a breakdown between relationship of $\dot{\varepsilon}_s$-σ near 600 MPa. Also precipitation on grain boundaries of the AR condition has occurred at 650 °C and 319-510 MPa, which help explain the low creep strain values. Considering the break point $n \cong 4$ calculated by Lagneborg and Bergman, which separates regions with different stress sensitivities, the effective values of stress exponent and activation energy were calculated for the Inconel 718 DA. The results of n_e, Q_e, internal stress, and TEM images suggest that the controlling mechanism of creep deformation is driven by dislocation-particle interaction, controlled by the particle shearing. As the temperature increases above 650 °C, the reduction of internal stress may contribute to the decrease of creep resistance of Inconel 718 DA, due to the transformation between γ'' and δ. The fracture images demonstrated that the failure mode of AR condition is due to transgranular fracture as well as mixed (intergranular-transgranular), and the Inconel 718 DA showed intergranular failure mode.

Acknowledgments

The authors acknowledge all the financial support gave from CAPES and technical/scientifical advice from LME/LNNano/CNPEM Process Number 15053. Especial thanks to Tarcila Sugahara and Fabiano Emmanuel Montoro. This work is dedicated to the memory of Prof. Carlos de Moura Neto.

References

1. T.S. Sims, N. Stoloff, and W.C. Hagel, *Superalloys II, High Temperature Materials for Aerospace and Industrial Power*, Willey, New York, 1987
2. F. Schubert, *Temperature and Time Dependent Transformation: Application to Heat Treatment of High Temperature Alloys*, ASM, Metals Park, 1983, p 3

3. G.R. Leverant and B.H. Kear, The Mechanism of Creep in Gamma Prime Precipitation-Hardened Nickel-Base Alloys at Intermediate Temperatures, *Metall. Trans.*, 1970, **1**, p 491–498
4. L.K. Singhal and M.L. Vaidya, Generation of Dislocations in a Precipitation Hardened Alloy, *Metall. Trans.*, 1970, **1**, p 1044–1045
5. J.K. Tien, B.H. Kear, and G.R. Leverant, On the High Activation Energy for Steady State Creep of Particle Strengthened Systems, *Scr. Metall.*, 1972, **6**, p 135–140
6. R. Lagneborg and B. Bergman, The Stress/Creep Rate Behavior of Precipitation-Hardened Alloys, *Met. Sci.*, 1976, **10**(1), p 20–28
7. L. Rémy, Precipitation Behavior and Creep Rupture of 706 Type Alloys, *Mater. Sci. Eng.*, 1979, **38**, p 227–239
8. O.D. Sherby and J. Weertman, Diffusion-Controlled Dislocation Creep: A Defense, *Acta Metall.*, 1979, **27**, p 387–400
9. K. Shiozawa and J.R. Weertman, The Nucleation of Grain Boundary Voids in a Nickel-Base Superalloy During High Temperature Creep, *Scr. Metall.*, 1982, **16**, p 735–739
10. B.F. Dyson and M. Mclean, Particle Coarsening, σ_0 and Tertiary Creep, *Acta Metall.*, 1983, **31**, p 17–27
11. O.D. Sherby and E.M. Taleff, Influence of Grain Size, Solute Atoms and Second-Phase Particles on Creep Behavior of Polycrystalline Solids, *Mater. Sci. Eng. A*, 2002, **A322**, p 89–99
12. H. De Cicco, M.I. Luppo, L.M. Gribaudo, and J. Ovejero-García, Microstructural Development and Creep Behavior in A286 Superalloy, *Mater. Charact.*, 2004, **52**, p 85–92
13. A. Soula, Y. Renollet, D. Boivin, J.-L. Pouchou, D. Locq, P. Caron, and Y. Bréchet, Analysis of High-Temperature Creep Deformation in a Polycrystalline Nickel-Base Superalloy, *Mater. Sci. Eng. A*, 2009, **A510–511**, p 301–306
14. R. Merabtine, J.P. Dallas, and M. Cornet, Creep Strengthening of Ni3(Al, Si) Intermetallic Alloy by Ductile Precipitates, *Intermetallics*, 2005, **13**, p 179–186
15. S. Li, J. Tao, T. Sugui, and H. Zhuangqi, Influence of Precipitate Morphology on Tensile Creep of a Single Crystal Nickel-Base Superalloy, *Mater. Sci. Eng. A*, 2007, **454–455**, p 461–466
16. A.A. Tavassoli, On the Anomalous Stress-Dependence of Creep Rate in Precipitation Strengthened Alloys, *Nucl. Eng. Des.*, 1979, **54**, p 279–287
17. B. Pieraggi and J.F. Uginet, *Superalloys 718, 625, 706 and Various Derivatives*, TMS, Warrendale, 1994, p 535–544
18. W.R. Sun, H.R. Guan, M. Wang, Z.G. Wang, L.F. Huang, and Z.Q. Hu, *Superalloys 718, 625, 706 and Various Derivatives*, TMS, Warrendale, 2005, p 399–407
19. X. Xie, Q. Liang, J. Dong, W. Meng, and Z. Xu, *Superalloys 718, 625, 706 and Various Derivatives*, TMS, Warrendale, 1994, p 711–720
20. G.D. Smith and S.J. Patel, *Superalloys 718, 625, 706 and Various Derivatives*, TMS, Warrendale, 2005, p 135–154
21. S. Azadian, L.-Y. Wei, and R. Warren, Delta Phase Precipitation in Inconel 718, *Mater. Charact.*, 2004, **53**, p 7–16
22. Z.F. Zhou and B.A. Parker, On the High-Stress Region Stress Exponent During Creep, *Scr. Metall. Mater.*, 1995, **32**, p 1889–1893
23. C.-M. Kuo, Y.-T. Yang, H.-Y. Bor, C.-N. Wei, and C.-C. Tai, Aging Effects on the Microstructure and Creep Behavior of Inconel 718 Superalloy, *Mater. Sci. Eng. A*, 2009, **A510–511**, p 289–294
24. American Society for Testing and Materials, E21-05, *Standard Test Methods for Elevated Temperature Tension Tests of Metallic Materials*, ASTM, Philadelphia, 2005
25. American Society for Testing and Materials, E139-11, *Standard Practice for Conducting Creep, Creep-Rupture and Stress-Rupture Tests of Metallic Materials*, ASTM, Philadelphia, 2011
26. Heat Treater's Guide, *Practices and Procedures for Nonferrous Alloys*, ASM International, The Materials Information Society, Materials Park, 1996
27. D.A.P. Reis, C.R.M. Silva, M.C.A. Nono, M.J.R. Barboza, F. Piorino-Neto, and E.A.C. Perez, Effect of Environment on the Creep Behavior of the Ti-6Al-4V Alloy, *Mater. Sci. Eng. A*, 2005, **399**, p 276–280
28. F.R.N. Nabarro and H.L. De Villiers, *The Physics of Creep*, Taylor and Francis Ltd., London, 1995
29. B. Kaplan, A. Blomqvist, C. Arhammar, M. Selleby, and S. Norgren, Structural Determination of $(Cr,Co)_7C_3$. *Proceedings of the 18th Plansee Seminar*, Reutte, Austria, 2013, pp. HM104/1–HM104/12
30. J.R. Davis, *ASM Specialty Handbook: Nickel, Cobalt and Their Alloys*, ASM International, Materials Park, 2000
31. M.F. Ashby, C. Gandhi, and D.M.R. Taplin, Fracture-Mechanism Maps and Their Construction for f.c.c. Metals and Alloys, *Acta Mater.*, 1979, **27**, p 699–729
32. Y. Han and M.C. Chaturvedi, Steady State Creep Deformation of Superalloy Inconel 718, *Mater. Sci. Eng.*, 1987, **89**, p 25–33
33. W. Chen and M.C. Chaturvedi, The Effect of Grain Boundary Precipitates on the Creep Behavior of Inconel 718, *Mater. Sci. Eng. A*, 1994, **183**, p 81–89
34. D.F. Paulonis, J.M. Oblak, and D.S. Duvall, Precipitation in Nickel-Base Alloy 718, *Trans. ASM*, 1969, **62**(3), p 611–622
35. R. Cozar and A. Pineau, Morphology of y' and y" Precipitates and Thermal Stability of Inconel 718 Type Alloys, *Metall. Trans.*, 1973, **4**(1), p 47–59
36. G. Venkataraman and F. Cosandey, Creep Behavior of Ni-Cr Alloys with Trace Additions of Cerium, *Mater. Sci. Eng.*, 1987, **93**, p 175–179